

Abelian Higgs Hair for Rotating and Charged Black Holes

A. M. Ghezelbash¹ and R. B. Mann²
Department of Physics, University of Waterloo,
Waterloo, Ontario N2L 3G1, CANADA

December 25, 2018

Abstract

We show that the Abelian Higgs field equations in the background of the four dimensional Kerr-AdS and Reissner-Nordstrom-AdS black holes have a vortex line solution. These solutions, which have axial symmetry, are generalization of the Nielsen-Olesen string. By the numerical study of the field equations in each case, we show that black holes could support the Abelian Higgs field as their Abelian hair. Also, we consider the self gravity of the Abelian Higgs field both in the Kerr-AdS and Reissner-Nordstrom-AdS black hole backgrounds and show that the effect of string as a black hole hair is to induce a deficit angle in the corresponding black hole metrics.

¹Email: amasoud@avatar.uwaterloo.ca

² Email: mann@avatar.uwaterloo.ca

1 Introduction

The conjecture that the only long-range information associated with the endpoint of gravitational collapse is that of its total mass, angular momentum and electric charge is referred to as the no-hair conjecture of black holes [1]. Much work has been carried out over the years on this conjecture, either upholding it in certain instances (e.g. scalar fields [2]) or challenging it in others, such as painting Yang-Mills, quantum hair [3] or Nielsen-Olesen vortices [4] on black holes. In fact the uniqueness of the classical no-hair theorems is a qualified uniqueness[5], incorporating additional criteria associated with stability, non trivial topology, and the possibility of field configurations on the horizon (referred to as ‘dressing’), and one must be quite specific about what is meant by ‘hair’ [4]. The study of Nielsen-Olesen vortices in the background of the charged black holes was done in [6],[7],[8] and [9].

Virtually all efforts in this area have been concerned with asymptotically flat spacetimes, and it is only recently that extensions to other types of asymptotia have been considered. Scalar fields minimally coupled to gravity cannot provide hair for asymptotically de Sitter black holes [10], but can do so if the spacetime is asymptotically anti de Sitter (AdS) [11]. A solution to the $SU(2)$ Einstein-Yang-Mills equations that describes a stable Yang-Mills hairy asymptotically AdS black hole has been shown to exist [3]. In a recent paper with Dehghani we have shown that the $U(1)$ Higgs field equations have a vortex solution in both four dimensional AdS spacetime [12] and AdS-Schwarzschild backgrounds [13].

In this paper we extend our investigation of possible vortex hair for non-asymptotically flat black holes to include rotation and charge. Specifically, we seek solutions of the Abelian-Higgs field equations in the four dimensional rotating Kerr-AdS and Reissner-Nordstrom-AdS black hole backgrounds. Although an analytic solution to these equations appears to be intractable, we confirm by numerical calculation that Kerr-AdS and Reissner-Nordstrom-AdS black holes could support a long range vortex (or cosmic string) as a form of stable hair.

In section two, we solve numerically the Abelian-Higgs equations in the Kerr-AdS background for different values of the cosmological constant and black hole rotation parameter. Also, in this section, we consider the Abelian-Higgs equations in the limiting case of Kerr-AdS background with cosmological constant to be zero, yielding the vortex equation in the Kerr black hole background. In section three, we repeat this calculation for a Reissner-Nordstrom-AdS background for different values of the black hole charge. In the limiting case of Reissner-Nordstrom-AdS black hole with cosmological constant to be zero, our solution is in good agreement with the previous obtained results [9]. Then in section four, by studying the behaviour of the string energy-momentum tensor, we find the effect of the vortex self gravity on the above mentioned black hole backgrounds. We give some closing remarks in the final section.

2 Abelian Higgs Vortex in Kerr–AdS Black Hole

The Abelian Higgs Lagrangian is

$$\mathcal{L}(\Phi, A_\mu) = -\frac{1}{2}(\mathcal{D}_\mu \Phi)^\dagger \mathcal{D}^\mu \Phi - \frac{1}{16\pi} \mathcal{F}_{\mu\nu} \mathcal{F}^{\mu\nu} - \xi(\Phi^\dagger \Phi - \eta^2)^2 \quad (1)$$

where Φ is a complex scalar Klein-Gordon field, $\mathcal{F}_{\mu\nu}$ is the field strength of the electromagnetic field A_μ and $\mathcal{D}_\mu = \nabla_\mu + ieA_\mu$ in which ∇_μ is the covariant derivative in a spacetime with metric $g_{\mu\nu}$. We employ Planck units $G = \hbar = c = 1$ which implies that the Planck mass is equal to unity, and write the Kerr-AdS black hole metric in the analogue of Boyer-Lindquist coordinates

$$ds^2 = -\frac{\Delta_r}{\rho^2} \left(dt - \frac{a}{\Sigma} \sin^2 \theta d\varphi\right)^2 + \frac{\rho^2}{\Delta_r} dr^2 + \frac{\rho^2}{\Delta_\theta} d\theta^2 + \frac{\Delta_\theta \sin^2 \theta}{\rho^2} \left(ad\varphi - \frac{r^2 + a^2}{\Sigma} d\varphi\right)^2 \quad (2)$$

where

$$\begin{aligned} \Delta_r &= (r^2 + a^2)\left(1 + \frac{r^2}{l^2}\right) - 2mr \\ \Delta_\theta &= 1 - \frac{a^2 \cos^2 \theta}{l^2} \\ \Sigma &= 1 - \frac{a^2}{l^2} \end{aligned} \quad (3)$$

and $\rho^2 = r^2 + a^2 \cos^2 \theta$. The parameter m is related to the mass of the black hole M by

$$M = \frac{ml}{\left(1 - \frac{a^2}{l^2}\right)^2}$$

and a to the angular momentum J by

$$J = \frac{am}{\left(1 - \frac{a^2}{l^2}\right)^2}$$

The cosmological constant Λ is equal to $\frac{-3}{l^2}$. The metric (2) is valid only where $|a| < l$ and is singular where $|a| = l$. If $m > 0$, Δ_r has at most two real roots and the event horizon is located at $r = r_H$, the largest real root of the equation $\Delta_r = 0$. If roots are not real, then the spacetime described by the metric (2) is a naked singularity. As in the non-rotating case [13], we define the real fields $X(x^\mu), \omega(x^\mu), P_\mu(x^\nu)$ via the following equations

$$\begin{aligned} \Phi(x^\mu) &= \eta X(x^\mu) e^{i\omega(x^\mu)} \\ A_\mu(x^\nu) &= \frac{1}{e} (P_\mu(x^\nu) - \nabla_\mu \omega(x^\mu)) \end{aligned} \quad (4)$$

from which we can rewrite the Lagrangian (1) and the equations of motion in terms of these fields as

$$\mathcal{L}(X, P_\mu) = -\frac{\eta^2}{2} (\nabla_\mu X \nabla^\mu X + X^2 P_\mu P^\mu) - \frac{1}{16\pi e^2} F_{\mu\nu} F^{\mu\nu} - \xi \eta^4 (X^2 - 1)^2 \quad (5)$$

$$\begin{aligned} \nabla_\mu \nabla^\mu X - X P_\mu P^\mu - 4\xi \eta^2 X (X^2 - 1) &= 0 \\ \nabla_\mu F^{\mu\nu} - 4\pi e^2 \eta^2 P^\nu X^2 &= 0 \end{aligned} \quad (6)$$

where $F^{\mu\nu} = \nabla^\mu P^\nu - \nabla^\nu P^\mu$ is the field strength of the corresponding gauge field P^μ .

Provided the field ω is not single valued, the resultant solutions contain physical information and are referred to as vortex solutions [14]. The requirement that Φ be single-valued implies that the line integral of ω over any closed loop is $\pm 2\pi n$ where n is an integer. Through such a closed loop the flux of electromagnetic field Φ_H is quantized with quanta $2\pi/e$.

We seek a vortex solution for the Abelian Higgs Lagrangian (5) in the background of Kerr-AdS black hole. This solution can be interpreted as a string piercing to the black hole (2). Considering the static case of winding number N with the gauge choice,

$$P_\mu(r, \theta) = (0; 0, 0, NP(r, \theta)) \quad (7)$$

and rescaling

$$\varkappa \rightarrow \frac{\varkappa}{\sqrt{\xi}\eta} \quad (8)$$

where $\varkappa = r, l, m$, the equations of motion (6) are

$$\begin{aligned} & \frac{(r^2+l^2)(r^2+a^2)-2mrl^2}{l^2(r^2+a^2\cos^2\theta)} \frac{\partial^2 X(r, \theta)}{\partial r^2} + 2 \frac{2r^3+r(l^2+a^2)-ml^2}{l^2(r^2+a^2\cos^2\theta)} \frac{\partial X(r, \theta)}{\partial r} + \frac{l^2-a^2\cos^2\theta}{l^2(r^2+a^2\cos^2\theta)} \frac{\partial^2 X(r, \theta)}{\partial \theta^2} + \cot\theta \frac{l^2+2a^2-3a^2\cos^2\theta}{l^2(r^2+a^2\cos^2\theta)} \frac{\partial X(r, \theta)}{\partial \theta} \\ & + \frac{(a-l)^2(a+l)^2(r^4+(r^2+a^2\cos^2\theta)(a^2+l^2)-a^4\cos^4\theta+2mrl^2)}{l^2\sin^2\theta(r^2+a^2\cos^2\theta)(a^2\cos^2\theta-l^2)(r^4+r^2(a^2+l^2)+a^2l^2-2mrl^2)} N^2 X(r, \theta) P(r, \theta)^2 - \frac{1}{2} X(r, \theta) (X(r, \theta)^2 - 1) = 0 \quad (9) \\ & - \frac{(r^2+l^2)(r^2+a^2)-2mrl^2}{l^2(r^2+a^2\cos^2\theta)} \frac{\partial^2 P(r, \theta)}{\partial r^2} - 2 \frac{(a^2+r^2)(r^5+2a^2\cos^2\theta r^3+ml^2r^2+a^4\cos^4\theta r-a^2ml^2\cos^2\theta)}{l^2(r^2+a^2\cos^2\theta)^3} \frac{\partial P(r, \theta)}{\partial r} + \frac{a^2\cos^2\theta-l^2}{l^2(r^2+a^2\cos^2\theta)} \frac{\partial^2 P(r, \theta)}{\partial \theta^2} \\ & + \cot\theta \frac{r^4(l^2-2a^2+a^2\cos^2\theta)+2a^2r^2(l^2\cos^2\theta+a^2\cos^4\theta-2a^2\cos^2\theta)+4a^2ml^2\sin^2\theta r+a^4\cos^2\theta(l^2\cos^2\theta+a^2\cos^4\theta-2a^2)}{l^2(r^2+a^2\cos^2\theta)^3} \frac{\partial P(r, \theta)}{\partial \theta} \\ & + \alpha P(r, \theta) X^2(r, \theta) = 0 \quad (10) \end{aligned}$$

In the above relation (10), $\alpha = \frac{4\pi e^2}{\xi}$. The equations (10) and (9) in the special cases of $a = 0$ and $a = m = 0$ reduce to the equations of motion of the vortex in the Schwarzschild-AdS and AdS backgrounds respectively [13],[12]. Note that even for $m = 0$, no exact analytic solutions are known for equations (9) and (10).

We now proceed with a search for the existence of vortex solutions for the above coupled non linear partial differential equations. First, we consider the *thin* string with winding number one, in which one can assume $m \gg 1$. The thicker vortex and larger winding number will be discussed later in this section. Employing the ansatz

$$P(r, \theta) = P(\rho), \quad X(r, \theta) = X(\rho) \quad (11)$$

where $\rho = r \sin\theta$, we get the following equations:

$$\begin{aligned} & - \frac{a^2(\rho^4+r^4-3r^2\rho^2-\rho^2l^2)-r^4(l^2+\rho^2)+2rml^2\rho^2}{l^2(r^4+a^2(r^2-\rho^2))} \frac{d^2 X}{d\rho^2} - \frac{a^2(r^4-7r^2\rho^2+4\rho^4)-r^4(4\rho^2+l^2)+2\rho^2ml^2r}{\rho l^2(r^4+a^2(r^2-\rho^2))} \frac{dX}{d\rho} \\ & - \frac{1}{2} (X^3 - X) + f(r, \theta) N^2 X P^2 = 0 \quad (12) \end{aligned}$$

$$\frac{r^2(a^2 \cos^4 \theta - l^2) - \sin^2 \theta(r^4 + a^2 r^2 - 2mrl^2 + a^2 l^2)}{l^2(r^2 + a^2 \cos^2 \theta)} \frac{d^2 P}{d\rho^2} + \frac{g(r, \theta)}{l^2 \sin \theta (r^2 + a^2 \cos^2 \theta)^3} \frac{dP}{d\rho} - \alpha P X^2 = 0 \quad (13)$$

where the functions $f(r, \theta)$ and $g(r, \theta)$ are given by,

$$f(r, \theta) = \frac{r^2(a-l)^2(a+l)^2(a^4 \rho^2 r^2 - a^4 \rho^4 + a^2 r^6 + a^2 r^4 l^2 - a^2 \rho^2 l^2 r^2 - 2r^5 m l^2 + r^8 + l^2 r^6)}{\rho^2 l^2 \{r^4 + a^2(r^2 - \rho^2)\} \{r^2(a^2 - l^2) - a^2 \rho^2\} \{(r^2 + l^2)(r^2 + a^2) - 2mrl^2\}} \quad (14)$$

$$g(r, \theta) = -2 \sin^2 \theta r^7 + (6 \cos^4 \theta a^2 + l^2 - 5a^2 \cos^2 \theta - 2a^2) r^5 - 2ml^2 \sin^2 \theta r^4 + \{-4a^4 \cos^2 \theta (1 + \cos^2 \theta) + 2a^2 l^2 \cos^2 \theta + 6a^4 \cos^6 \theta\} r^3 - 2a^2 m l^2 (1 + 3 \cos^4 \theta - 4 \cos^2 \theta) r^2 + a^4 \cos^4 \theta (l^2 - 2a^2 + 2a^2 \cos^4 \theta - a^2 \cos^2 \theta) + 2a^4 m l^2 \sin^2 \theta \cos^2 \theta \quad (15)$$

When $a = 0$, the vortex solutions of the Abelian Higgs equations in flat spacetime (without a black hole) satisfy the $l \rightarrow \infty$ limit of equations up to errors which are proportional to the $\frac{m\rho^2}{r^3} \approx \frac{m}{r^3}$ [12]. These errors are very tiny far from the black hole horizon, whereas near the horizon $r \approx r_H = 2m$, they are of the order of $\frac{1}{m^2}$, which is negligible for large mass black holes. This suggests that a string vortex solution could be painted to the horizon of a Schwarzschild black hole, and numerical calculations [4] have indeed shown the existence of vortex solutions of the Abelian Higgs equations in this background.

The situation is somewhat different for finite l . For $a = 0$ (and $l \neq 0$) we showed in our previous paper [12] that the Abelian Higgs equations of motion in the background of Anti-de-Sitter spacetime ((12) and (13) in the limit of $a = 0$ and $m = 0$) have vortex solutions (denoted by X_0 and P_0) with core radius $\rho \approx O(1)$. The functions X_0 and P_0 satisfy eqs. (12) and (13) up to errors which are proportional to $\frac{m\rho^2}{r^3} \approx \frac{m}{r^3}$. Although these errors go to zero far from the black hole, for a large mass black hole, $r \approx r_H \approx m^{1/3}$, the term $\frac{m}{r^3}$ is at least of the order of unity, and so the possibility of obtaining a string vortex solution for finite l in this background is unclear.

By numerically solving eqs. (12,13) in the $a = 0$ case we have shown that vortex solutions exist on, near and far from the horizon of the AdS-Schwarzschild black hole for various winding numbers and different values of l [13]. As in the asymptotically flat case the results indicate that increasing the winding number yields a greater vortex thickness. Furthermore as l decreases the black hole becomes completely covered by a vortex of decreasingly large winding number. Also, for a vortex with definite winding number, the string core decreases with decreasing l , but the ratio of string core to the size of the black hole horizon increases. The X and P fields less rapidly approach their respective maximum and minimum values at larger angles as l decreases.

For finite values of the rotation parameter a , equations (12) and (13) are considerably more complicated than in the $a = 0$ case. To obtain numerical solutions of (10) and (9) outside the black hole horizon we must first select appropriate boundary conditions. At the large distance from the horizon physical considerations motivate a clear choice: we demand that the $a \neq 0$ solutions approach the solutions of the vortex equations in pure AdS spacetime given in ref. [12]. This means that we demand $X \rightarrow 1$ and $P \rightarrow 0$ as ρ goes to infinity. On the symmetry axis of

the string and beyond the radius of horizon r_H , i.e. $\theta = 0$ and $\theta = \pi$, we take $X \rightarrow 0$ and $P \rightarrow 1$. Finally, on the horizon, we initially take $X = 0$ and $P = 1$.

We then employ a polar grid of points (r_i, θ_j) , where r goes from r_H to some large value of r (r_∞) which is much greater than r_H and θ runs from 0 to π . We use the finite difference method and rewrite the non linear partial differential equation (9) and (10) as

$$A_{ij}X_{i+1,j} + B_{ij}X_{i-1,j} + C_{ij}X_{i,j+1} + D_{ij}X_{i,j-1} + E_{ij}X_{i,j} = F_{ij} \quad (16)$$

$$A'_{ij}P_{i+1,j} + B'_{ij}P_{i-1,j} + C'_{ij}P_{i,j+1} + D'_{ij}P_{i,j-1} + E'_{ij}P_{i,j} = F'_{ij} \quad (17)$$

where $X_{ij} = X(r_i, \theta_j)$ and $P_{ij} = P(r_i, \theta_j)$. For the interior grid points and horizon grid points, the coefficients A_{ij}, \dots, F'_{ij} can be straightforwardly determined from the corresponding continued differential equations (9) and (10). The form of the coefficients is somewhat complicated, and we so relegate them to an appendix.

Using the well known successive overrelaxation method [15] for the above mentioned finite difference equations, we obtain the values of X and P fields inside the grid, which we denote them by $X^{(1)}$ and $P^{(1)}$. Then by calculating the r -gradients of X and P just outside the horizon and iterating the finite difference equations on the horizon, we get the new values of X and P fields on the horizon points. Then these new values of X and P fields are used as the new boundary condition on the horizon for the next step in obtaining the values of X and P fields inside the grid which could be denoted by $X^{(2)}$ and $P^{(2)}$. Repeating this procedure, the value of the each field in the $(n+1)$ -th iteration is related to the n -th iteration by

$$X_{ij}^{(n+1)} = X_{ij}^{(n)} - \omega \frac{\zeta_{ij}^{(n)}}{E_{ij}^{(n)}} \quad (18)$$

$$P_{ij}^{(n+1)} = P_{ij}^{(n)} - \omega \frac{\varsigma_{ij}^{(n)}}{E'_{ij}^{(n)}} \quad (19)$$

where the residual matrices $\zeta_{ij}^{(n)}$ and $\varsigma_{ij}^{(n)}$ are the differences between the left and right hand sides of the equations (16) and (17) respectively, evaluated in the n -th iteration and ω is the overrelaxation parameter. The iteration is performed many times to some value $n = K$, such that $\sum_{i,j} |X_{ij}^{(K)} - X_{ij}^{(K-1)}| < \varepsilon$ and $\sum_{i,j} |P_{ij}^{(K)} - P_{ij}^{(K-1)}| < \varepsilon$ for a given error ε . It is a matter of trial and error to find the value of ω that yields the most rapid convergence.

Some typical results of this calculation are displayed in figures (1), (2) and (4),(5), (6) for different values of $l = 5$ and $l = 10$, respectively. In the first case, we consider both $a = 0$ and $a = 3$ and in the second case, we consider $a = 0, 5, 8$. For $l = 5$, the black hole mass is taken to be the constant value $m = 10$ whereas for $l = 10$ the mass is taken to be $m = 20$. In $l = 5$, the horizon is located in $r_H = 6.89$ for $a = 0$ and $r_H = 6.30$ for $a = 3$. Also, for the case of $l = 10$, the horizon for different values of $a = 0, 5, 8$ are $r_H = 13.79, 12.98, 11.57$ respectively. The diagrams

(1) and (4) when $a = 0$ are exactly the same as the results of [13] for the AdS-Schwarzschild black hole.

We notice that by increasing the rotation parameter a from 0 to 3, the string core decreases slightly in the $l = 5$ Kerr-AdS black hole. Figure (3) shows explicitly the string core decreasing as the rotation parameter increases. Figure (7) illustrates for $l = 10$ a similar decrease of the string core as a increases from 0 to 5 and then to 8, respectively. Similar calculation for the string with larger winding numbers in a Kerr-AdS black hole with definite parameters l, a , shows that increasing the winding number yields a greater vortex thickness.

It is interesting to consider here the Abelian Higgs vortex in the Kerr black hole background. The Kerr metric is a special case of (2) in the limit $l \rightarrow \infty$. The metric is given by,

$$ds^2 = -\frac{\Delta}{\rho^2}(dt - a \sin^2 \theta d\varphi)^2 + \frac{\rho^2}{\Delta}dr^2 + \rho^2 d\theta^2 + \frac{\sin^2 \theta}{\rho^2}((r^2 + a^2)d\varphi - a dt)^2 \quad (20)$$

where $\Delta = r^2 - 2mr + a^2$. The horizon is located in $r_H = m + \sqrt{m^2 - a^2}$. The equations of motion for the X and P fields can be obtained from the equations (9) and (10) in the limit of $l \rightarrow \infty$. They are,

$$\begin{aligned} & \frac{r^2 + a^2 - 2mr}{r^2 + a^2 \cos^2 \theta} \frac{\partial^2 X(r, \theta)}{\partial r^2} + 2 \frac{r - m}{r^2 + a^2 \cos^2 \theta} \frac{\partial X(r, \theta)}{\partial r} + \frac{1}{r^2 + a^2 \cos^2 \theta} \frac{\partial^2 X(r, \theta)}{\partial \theta^2} + \cot \theta \frac{1}{r^2 + a^2 \cos^2 \theta} \frac{\partial X(r, \theta)}{\partial \theta} \\ & - \frac{r^2 + a^2 \cos^2 \theta + 2mr}{r^2 + a^2 - 2mr} N^2 X(r, \theta) P(r, \theta)^2 - \frac{1}{2} X(r, \theta) (X(r, \theta)^2 - 1) = 0 \end{aligned} \quad (21)$$

$$\begin{aligned} & -\frac{r^2 + a^2 - 2mr}{r^2 + a^2 \cos^2 \theta} \frac{\partial^2 P(r, \theta)}{\partial r^2} - 2m \frac{(a^2 + r^2)(r^2 - a^2 \cos^2 \theta)}{(r^2 + a^2 \cos^2 \theta)^3} \frac{\partial P(r, \theta)}{\partial r} - \frac{1}{r^2 + a^2 \cos^2 \theta} \frac{\partial^2 P(r, \theta)}{\partial \theta^2} \\ & + \cot \theta \left(\frac{1}{r^2 + a^2 \cos^2 \theta} + 4 \frac{rma^2 \sin^2 \theta}{(r^2 + a^2 \cos^2 \theta)^3} \right) \frac{\partial P(r, \theta)}{\partial \theta} + \alpha P(r, \theta) X^2(r, \theta) = 0 \end{aligned} \quad (22)$$

We solve the differential equations (21) and (22) numerically, using the same approach employed in solving (9) and (10). Some typical results of the calculation are displayed in figures (8), (9) and (10). In these calculations, we consider a string with unit winding number in the background (20) with $a = 0, 5$ and $a = 9$. The black hole mass is taken to be the constant value $m = 10$. The horizon is located in $r_H = 20$ for $a = 0$ and $r_H = 18.66, 14.36$ for $a = 5, 9$ respectively.

The figures in (8), when $a = 0$ are exactly the same as the results of the Schwarzschild black hole [4],[12]. We note that despite the change of the rotation parameter from 0 to 9, both the X and P contours do not change considerably. In fact, as the diagrams in figure (11) show, only near the black hole horizon, we observe a very tiny change on the $X = 0.9$ and $P = 0.1$ contours. By increasing the rotation parameter, both the X and P contours decrease a little.

3 Abelian Higgs Vortex in Reissner-Nordstrom-AdS black hole

In this section, we consider the Abelian Higgs vortex Lagrangian (1) in the background of a charged black hole. The background metric is given by,

$$ds^2 = -\left(1 - \frac{2m}{r} + \frac{Q^2}{r^2} + \frac{r^2}{l^2}\right)dt^2 + \frac{1}{1 - \frac{2m}{r} + \frac{Q^2}{r^2} + \frac{r^2}{l^2}}dr^2 + r^2(d\theta^2 + \sin^2 \theta d\varphi^2) \quad (23)$$

Q is the total charge of black hole which measured by a far observer located at $r \gg 2M, Q$, and the black hole horizon r_H is located at the largest real root of the equation $r^4 + l^2 r^2 - 2ml^2 r + Q^2 l^2 = 0$. In the special case of $l \rightarrow \infty$, the horizon is located at $r_H = m + \sqrt{m^2 - Q^2}$. The Abelian Higgs Lagrangian is as the same as (1) with the real fields $X(x^\mu), \omega(x^\mu), P_\mu(x^\nu)$ again given by the relations (4), whose equations of motion are (5) and (6). The equations of motion derived from the Lagrangian for the $X(r, \theta)$ and $P(r, \theta)$ fields after rescaling of coordinates in the background (23) are

$$\begin{aligned} & \left(1 - \frac{2m}{r} + \frac{Q^2}{r^2} + \frac{r^2}{l^2}\right) \frac{\partial^2 X(r, \theta)}{\partial r^2} + \frac{2}{r} \left(1 - \frac{m}{r} + \frac{2r^2}{l^2}\right) \frac{\partial X(r, \theta)}{\partial r} + \frac{1}{r^2} \frac{\partial^2 X(r, \theta)}{\partial \theta^2} + \frac{1}{r^2} \frac{\partial X(r, \theta)}{\partial \theta} \cot \theta - \frac{1}{2} (X^3(r, \theta) \\ & - X(r, \theta)) - N^2 \frac{X(r, \theta) P^2(r, \theta)}{r^2 \sin^2 \theta} = 0 \end{aligned} \quad (24)$$

$$\begin{aligned} & \left(1 - \frac{2m}{r} + \frac{Q^2}{r^2} + \frac{r^2}{l^2}\right) \frac{\partial^2 P(r, \theta)}{\partial r^2} + \frac{2}{r} \left(\frac{m}{r} + \frac{r^2}{l^2} - \frac{Q^2}{r^2}\right) \frac{\partial P(r, \theta)}{\partial r} + \frac{1}{r^2} \frac{\partial^2 P(r, \theta)}{\partial \theta^2} - \frac{\cot \theta}{r^2} \frac{\partial P(r, \theta)}{\partial \theta} \\ & - \alpha P(r, \theta) X^2(r, \theta) = 0 \end{aligned} \quad (25)$$

We note that in the special case $Q = 0$, the equations of motion (24) and (25) reduce to the equations of motion of the vortex in the background of AdS-Schwarzschild background studied in [13]. Also we note that in the special case of $l \rightarrow \infty$, the above mentioned equations reduce to the equations of motion in the background of the Reissner-Nordstrom black hole discussed in [6] and [7].

We consider the static case of a string solution with winding number one. Using the overrelaxation method described in section two, we solve numerically the equations of motion. A typical result for the string fields in the background of the Reissner-Nordstrom-AdS black hole with $l = 5$ and $Q = 5$ is presented in figure (12). As figure (13) shows, by increasing the parameter l from 3 to ∞ , the string core changes a little. Such a tiny increase of string core also has been observed in the case of AdS-Schwarzschild black hole by increasing the parameter l [13]. In the special case of $l \rightarrow \infty$, a typical solution of (24) and (25) for a Reissner-Nordstrom black hole with $m = 10$ and $Q = 5$ is shown in figure (14). In figure (15), the $X = 0.9$ and $P = 0.1$ contours are plotted for three different values of the charge parameter $Q = 0, 5, 10$. The last case corresponds to extremal case $Q = m = 10$. So, we observe that despite the smaller horizon radius for a black hole with more charge, the string core does not change drastically for the charged black holes for a wide range of the charge parameter $0 \leq Q \leq 10$. In the extremal case we find that an extremal horizon is indeed pierced by a thin string, confirming earlier computations carried out in refs. [8] and [9], and that the vortex flux is not expelled from the black hole. In these calculations, we have used a 600×700 grid in the (r, θ) directions, a much finer resolution than previous studies have employed [6, 7, 8, 9], respectively. Note that there are no values of Q or m for which the black hole becomes extremal in the asymptotically AdS case.

4 Vortex Self Gravity on the Kerr-AdS and Reissner-Nordstrom-AdS Black Holes

We now first consider the effect of the vortex on the Kerr-AdS black hole. As we have seen in [13], this is a formidable problem even for the simpler cases of the effect of the vortex on the AdS-Schwarzschild or Schwarzschild black hole backgrounds.

For the AdS-Schwarzschild black hole, it has been shown that the components of the energy-momentum tensor rapidly go to zero outside the core string, leading to a situation similar to that of pure AdS spacetime. A full study of the vortex self gravity in pure AdS spacetime has been carried out in ref. [13]. We assume for the present case that the thickness of the vortex is much smaller than all other relevant length scales and that the gravitational effects of the string are weak enough so that the linearized Einstein-Abelian Higgs differential equations are applicable. So, we consider a thin string with the winding number $N = 1$ in the Kerr-AdS background with $l = 5$. The analysis for $l = 10$ is similar. The rescaled diagonal components of the energy-momentum tensor are

$$T_{\mu\mu} = f_{\mu\mu}^{(r)} \left(\frac{\partial X}{\partial r} \right)^2 + g_{\mu\mu}^{(r)} \left(\frac{\partial P}{\partial r} \right)^2 + f_{\mu\mu}^{(\theta)} \left(\frac{\partial X}{\partial \theta} \right)^2 + g_{\mu\mu}^{(\theta)} \left(\frac{\partial P}{\partial \theta} \right)^2 + h_{1\mu\mu} (X^2 - 1)^2 + h_{2\mu\mu} X^2 P^2 \quad (26)$$

where the functions $f_{\mu\mu}^{(r)}, f_{\mu\mu}^{(\theta)}, g_{\mu\mu}^{(r)}, g_{\mu\mu}^{(\theta)}, h_{1\mu\mu}$ and $h_{2\mu\mu}$ are complicated functions of the coordinates (r, θ) . Their functional forms are presented in the appendix. In the figure (16) the behaviour of energy-momentum tensor components for a fixed value of z is shown. We have checked that the behaviour of the components other z directions is similar.

It is clear from these figures that the components of the energy-momentum tensor rapidly go to zero outside the core of the vortex, so the situation is similar to that of AdS-Schwarzschild spacetime. Performing the same calculation as in for pure AdS spacetime described in detail in [13], we obtain the following metric for the Kerr-AdS spacetime incorporating the effect of the vortex

$$ds^2 = -\frac{\Delta_r}{\rho^2} \left(dt - \frac{\alpha\beta}{\Sigma} \sin^2 \theta d\varphi \right)^2 + \frac{\rho^2}{\Delta_r} dr^2 + \frac{\rho^2}{\Delta_\theta} d\theta^2 + \frac{\Delta_\theta \sin^2 \theta}{\rho^2} \left(adt - \beta \frac{r^2 + a^2}{\Sigma} d\varphi \right)^2 \quad (27)$$

which β is a constant dependent on the different parameters of the black hole. The above metric describes a Kerr-AdS metric with a deficit angle. Also if we take the limiting case of $l \rightarrow \infty$, we get the following Kerr spacetime incorporated the effect of the string on it,

$$ds^2 = -\frac{\Delta}{\rho^2} (dt - a\gamma \sin^2 \theta d\varphi)^2 + \frac{\rho^2}{\Delta} dr^2 + \rho^2 d\theta^2 + \frac{\sin^2 \theta}{\rho^2} (\gamma(r^2 + a^2) d\varphi - adt)^2$$

in which γ is another constant that also depends on the different parameters of the Kerr black hole.

So, using a physical Lagrangian based model, we have established that the presence of the cosmic string induces a deficit angle in the Kerr-AdS and Kerr black holes metric. In the case of charged Reissner-Nordstrom-AdS black hole, the energy-momentum tensor also goes rapidly to zero outside the core string, so the above arguments are still applicable: the effect of the vortex on the background (23) simply multiplies the angle coordinate φ by a constant, inducing a deficit angle in the Reissner-Nordstrom black hole spacetime.

5 Conclusion

The effect of a vortex on pure AdS spacetime is to create a deficit angle in the metric in the thin vortex approximation. We have extended this result to the charged and stationary cases, establishing numerically that Abelian Higgs vortices of finite thickness can pierce the Kerr, Kerr-AdS, and Reissner-Nordstrom-AdS black hole horizons. These solutions could thus be interpreted as stable Abelian hair for these black holes.

We have obtained numerical solutions for various cosmological constants and rotation parameter for a string with winding number one. Our solutions in the limit $a \rightarrow 0$ coincide with the known solutions in the AdS-Schwarzschild spacetime. We found that by increasing the value of rotation parameter, the string core decreases. Inclusion of the self gravity of the vortex in the Kerr-AdS background metric was shown to induce a deficit angle in this metric. Also, we have obtained numerical solutions for a string with winding number one in the background of a charged black hole for different values of charge parameters. In this case even in the extremal case, the string core remains nearly as the same as the Schwarzschild black hole with the same mass. We observe that in the extremal case, just like the non-extremal case, the string can pierce to the charged black hole horizon and no flux expulsion occurs. So, in this paper, using a physical Lagrangian based model, we have established that cosmic string could be pierced to rotating and charged black holes and the presence of the string induces deficit angles in these black hole metrics.

Other interesting issues concern the development of a holographic description of the vortex solution in these spacetimes and extensions of the vortex solution to asymptotically de Sitter (dS) spacetimes. Work on these problems is in progress.

6 Appendix

Here we present the coefficients A_{ij}, \dots, F'_{ij} appear in the equations (16) and (17). Let us rename the coefficients of the $\frac{\partial^2 X(r, \theta)}{\partial r^2}, \frac{\partial X(r, \theta)}{\partial r}, \frac{\partial^2 X(r, \theta)}{\partial \theta^2}, \frac{\partial X(r, \theta)}{\partial \theta}$ and $X(r, \theta)$ (fifth term) appearing in the equation (9) by $X_{rr}, X_r, X_{\theta\theta}, X_\theta, X$ respectively. Also, we rename the coefficients of the $\frac{\partial^2 P(r, \theta)}{\partial r^2}, \frac{\partial P(r, \theta)}{\partial r}, \frac{\partial^2 P(r, \theta)}{\partial \theta^2}, \frac{\partial P(r, \theta)}{\partial \theta}$ appearing in the equation (10) by $P_{rr}, P_r, P_{\theta\theta}, P_\theta$ respectively. Then the coefficients A_{ij}, \dots, F_{ij} inside the grid points are given by the following relations,

$$\begin{aligned}
 A_{ij} &= \left\{ \frac{X_{rr}}{(\Delta r)^2} + \frac{X_r}{2\Delta r} \right\}_{r=r_i, \theta=\theta_j} \\
 B_{ij} &= \left\{ \frac{X_{rr}}{(\Delta r)^2} - \frac{X_r}{2\Delta r} \right\}_{r=r_i, \theta=\theta_j} \\
 C_{ij} &= \left\{ \frac{X_{\theta\theta}}{(\Delta \theta)^2} + \frac{X_\theta}{2\Delta \theta} \right\}_{r=r_i, \theta=\theta_j} \\
 D_{ij} &= \left\{ \frac{X_{\theta\theta}}{(\Delta \theta)^2} - \frac{X_\theta}{2\Delta \theta} \right\}_{r=r_i, \theta=\theta_j} \\
 E_{ij} &= \left\{ -2 \left(\frac{X_{rr}}{(\Delta r)^2} + \frac{X_{\theta\theta}}{(\Delta \theta)^2} \right) + \tilde{X} \right\}_{r=r_i, \theta=\theta_j} \\
 F_{ij} &= -\frac{1}{2} X_{ij} (X_{ij}^2 - 1)
 \end{aligned}$$

The coefficients A'_{ij}, \dots, D'_{ij} have the similar form as A_{ij}, \dots, D_{ij} with the replacements $X_{rr}, X_r, X_{\theta\theta}, X_\theta$ by $P_{rr}, P_r, P_{\theta\theta}, P_\theta$ and

$$E'_{ij} = -2 \left\{ \frac{X_{rr}}{(\Delta r)^2} + \frac{X_{\theta\theta}}{(\Delta \theta)^2} \right\}_{r=r_i, \theta=\theta_j} + \alpha X_{ij}^2$$

The coefficient F'_{ij} is equal to zero.

Here, we present also some of the functional form of the functions $f_{\mu\mu}^{(r)}, f_{\mu\mu}^{(\theta)}, g_{\mu\mu}^{(r)}, g_{\mu\mu}^{(\theta)}, h_{1\mu\mu}$ and $h_{2\mu\mu}$ which was appeared in the formula (26).

For example, we have

$$\begin{aligned} f_{tt}^{(r)} &= \frac{(r^2 l^2 + r^4 + a^2 l^2 + r^2 a^2 - 2mrl^2)(r^2 l^2 + r^4 + r^2 a^2 - 2mrl^2 + a^2 l^2 \cos^2 \theta + a^4 \cos^2 \theta - a^4 \cos^4 \theta)}{2l^4(a^2 \cos^2 \theta + r^2)^2} \\ f_{tt}^{(\theta)} &= \frac{(a^2 \cos^2 \theta - l^2)(-r^2 l^2 - r^4 - r^2 a^2 + 2mrl^2 - a^2 l^2 \cos^2 \theta - a^4 \cos^2 \theta + a^4 \cos^4 \theta)}{2l^4(a^2 \cos^2 \theta + r^2)^2} \\ g_{tt}^{(r)} &= \frac{(r^2 l^2 + r^4 + r^2 a^2 - 2mrl^2 + a^2 l^2 \cos^2 \theta + a^4 \cos^2 \theta - a^4 \cos^4 \theta)^2 (a^2 - l^2)^2}{2\alpha l^6 (a^2 \cos^2 \theta + r^2)^3 \sin^2 \theta (l^2 - a^2 \cos^2 \theta)} \\ g_{tt}^{(\theta)} &= \frac{(r^2 l^2 + r^4 + r^2 a^2 - 2mrl^2 + a^2 l^2 \cos^2 \theta + a^4 \cos^2 \theta - a^4 \cos^4 \theta)^2 (a^2 - l^2)^2}{2\alpha l^6 (a^2 \cos^2 \theta + r^2)^3 \sin^2 \theta (r^2 l^2 + r^4 + a^2 l^2 + r^2 a^2 - 2mrl^2)} \\ h_{1tt} &= \frac{(r^2 l^2 + r^4 + r^2 a^2 - 2mrl^2 + a^2 l^2 \cos^2 \theta + a^4 \cos^2 \theta \sin^2 \theta)}{l^2 (a^2 \cos^2 \theta + r^2)} \\ h_{2tt} &= \frac{(r^2 l^2 + r^4 + r^2 a^2 - 2mrl^2 + a^2 l^2 \cos^2 \theta + a^4 \cos^2 \theta \sin^2 \theta)(a^2 - l^2)^2}{2l^4 (a^2 \cos^2 \theta - l^2) \sin^2 \theta (a^2 \cos^2 \theta + r^2)^2 (r^2 l^2 + r^4 + a^2 l^2 + r^2 a^2 - 2mrl^2)} \end{aligned}$$

Other functions have similar complicated structures; we shall not present them here.

Acknowledgments

This work was supported by the Natural Sciences and Engineering Research Council of Canada.

References

- [1] R. Ruffini and J.A. Wheeler. *Phys. Today* **24**, 30 (1971).
- [2] D. Sudarsky, *Class. Quant. Grav.* **12**, 579 (1995).
- [3] E. Winstanley, *Class. Quant. Grav.* **16**, 1963 (1999).
- [4] A. Achúcarro, R. Gregory, K. Kuijken, *Phys. Rev.* **D52**, 5729 (1995).
- [5] P. Cruschiel, gr-qc/9402032 (unpublished).
- [6] A. Chamblin, J.M.A. Ashbourn-Chamblin, R. Emparan, A. Sornborger, *Phys. Rev.* **D58**, 124014 (1998).
- [7] A. Chamblin, J.M.A. Ashbourn-Chamblin, R. Emparan, A. Sornborger, *Phys. Rev. Lett.* **80**, 4378 (1998).
- [8] F. Bonjour, R. Gregory, *Phys. Rev. Lett.* **81**, 5034 (1998).
- [9] F. Bonjour, R. Emparan, R. Gregory, *Phys. Rev.* **D59**, 84022 (1999).
- [10] T. Torii, K. Maeda and M. Narita, *Phys. Rev.* **D59**, 064027 (1999).

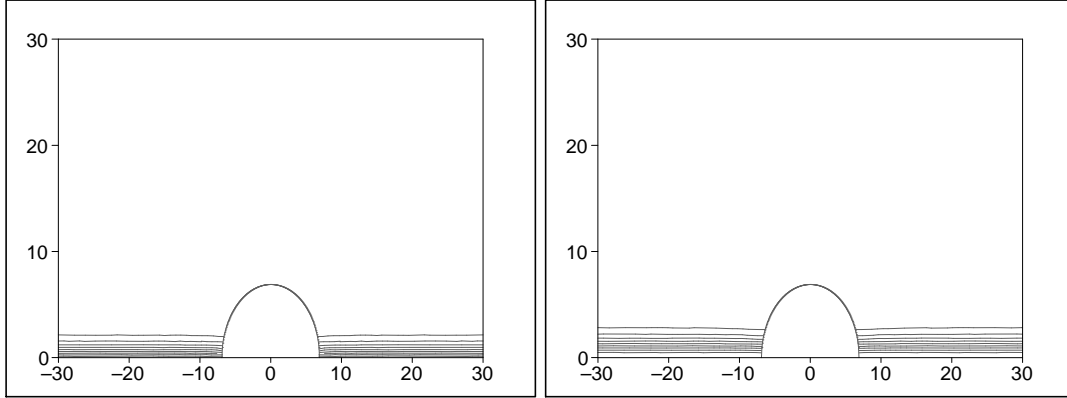


Figure 1: X and P contours (X and P increase from 0.1 to 0.9 upward and downward respectively) in the background of Kerr-AdS black hole with $l = 5$ and $a = 0$. The mass of black hole is equal to 10 and horizon is located in $r_H = 6.89$.

- [11] T. Torii, K. Maeda and M. Narita, *Phys. Rev.* **D64**, 044007 (2001).
- [12] M.H. Dehghani, A.M. Ghezelbash and R.B. Mann, hep-th/0105134.
- [13] M.H. Dehghani, A.M. Ghezelbash and R.B. Mann, hep-th/0107224.
- [14] H.B. Nielsen and P.Olesen, *Nucl. Phys.* **B61**, 45 (1973).
- [15] W. H. Press, S. A. Teukolsky, W. T. Vetterling and B. P. Flannery, "*Numerical Recipes in FORTRAN*", Cambridge University Press (1992).

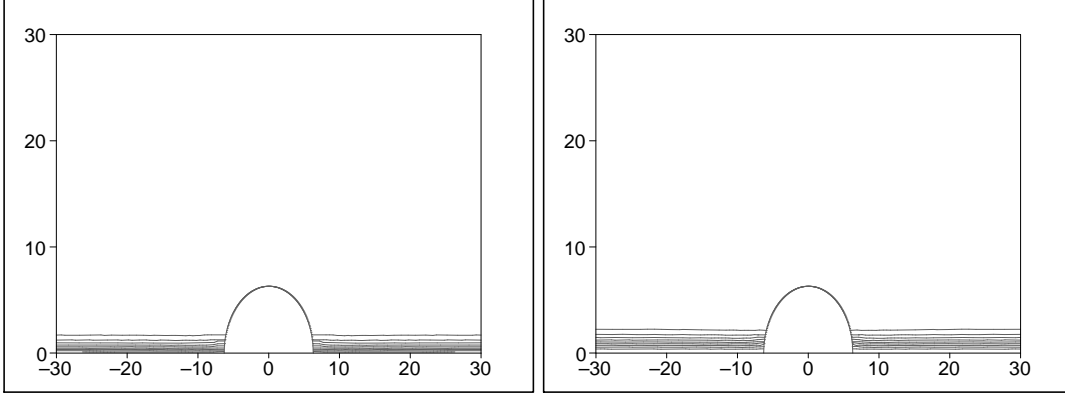


Figure 2: X and P contours (X and P increase from 0.1 to 0.9 upward and downward respectively) in the background of Kerr-AdS black hole with $l = 5$ and $a = 3$. The mass of black hole is equal to 10 and horizon is located in $r_H = 6.30$.

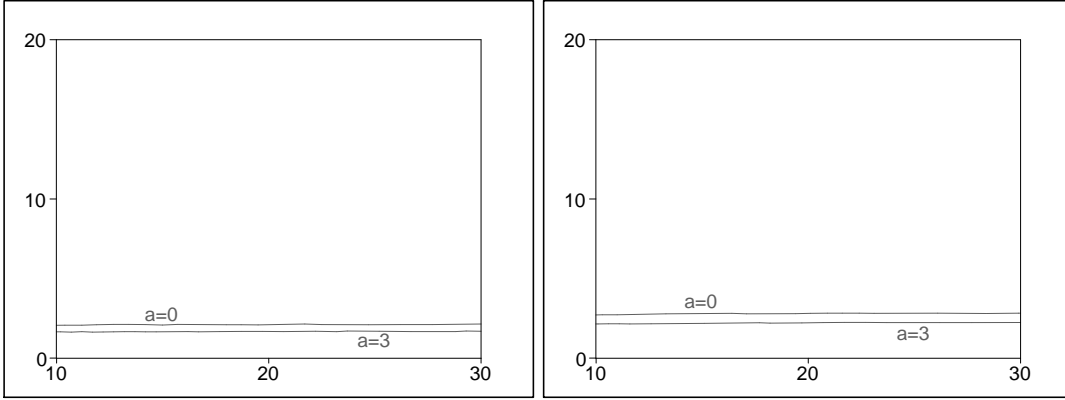


Figure 3: $X = 0.9$ and $P = 0.1$ contours in the presence of $l = 5$ Kerr-AdS black hole for different values of the rotation parameter $a = 0, 3$. The black hole horizon is located off to the left of the figure at $r_H = 6.89, 6.30$ respectively.

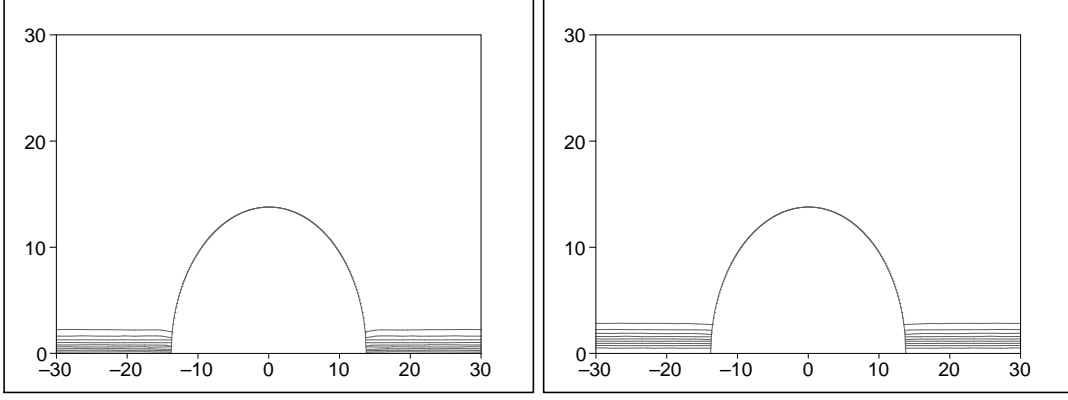


Figure 4: X and P contours (X and P increase from 0.1 to 0.9 upward and downward respectively) in the background of Kerr-AdS black hole with $l = 10$ and $a = 0$. The mass of black hole is equal to 20 and horizon is located in $r_H = 13.79$.

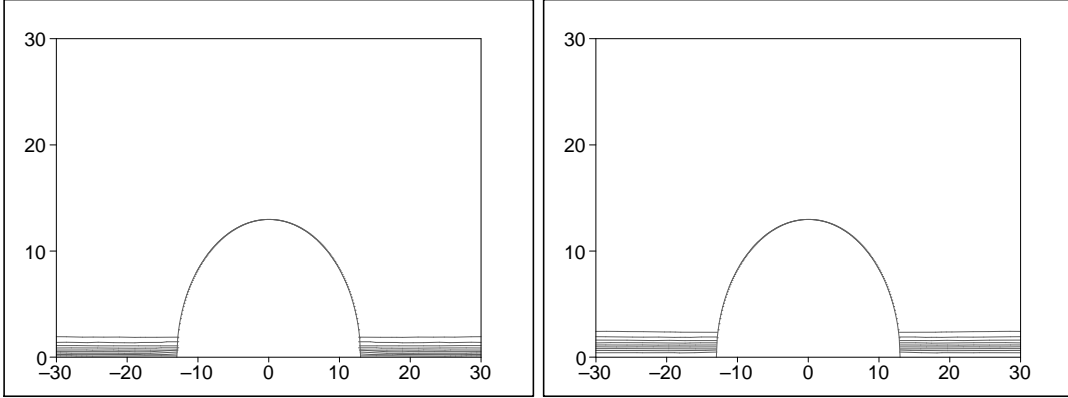


Figure 5: X and P contours (X and P increase from 0.1 to 0.9 upward and downward respectively) in the background of Kerr-AdS black hole with $l = 10$ and $a = 5$. The mass of black hole is equal to 20 and horizon is located in $r_H = 12.98$.

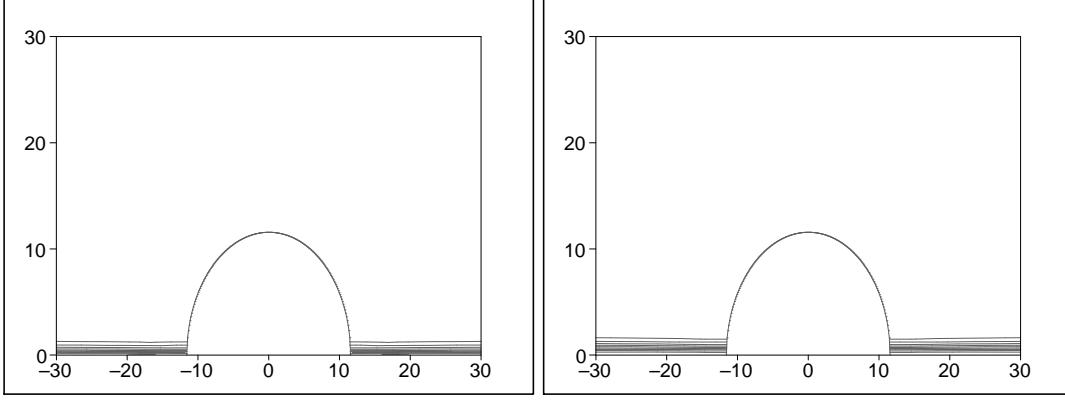


Figure 6: X and P contours (X and P increase from 0.1 to 0.9 upward and downward respectively) in the background of Kerr-AdS black hole with $l = 10$ and $a = 8$. The mass of black hole is equal to 20 and horizon is located in $r_H = 11.57$.

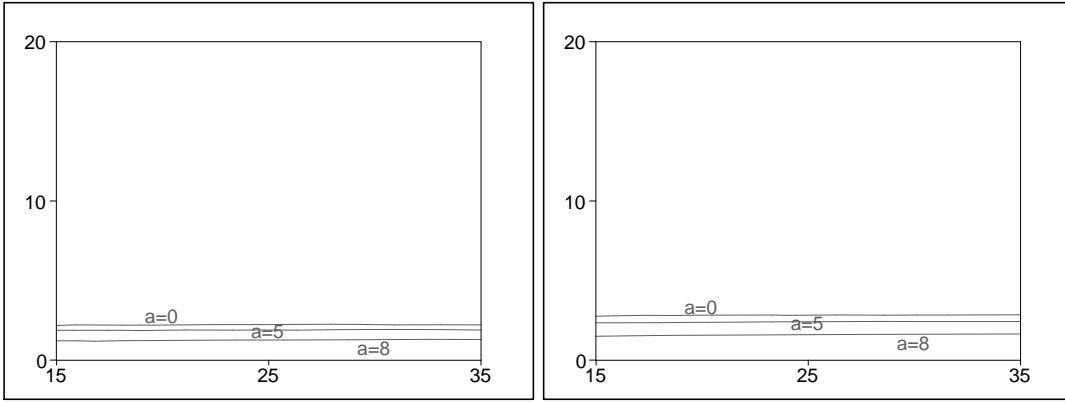


Figure 7: $X = 0.9$ and $P = 0.1$ contours in the presence of $l = 10$ Kerr-AdS black hole for different values of the rotation parameter $a = 0, 5, 8$. The black hole horizon is located off to the left of the figure at $r_H = 13.79, 12.98, 11.57$ respectively.

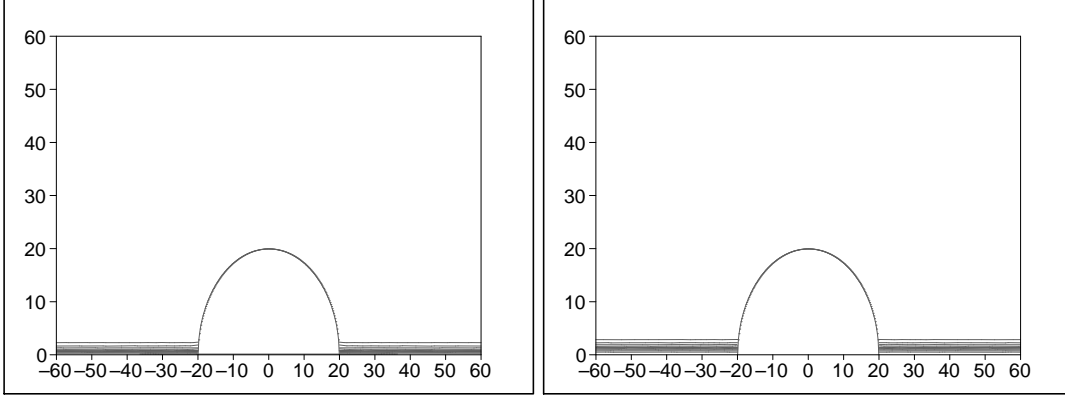


Figure 8: X and P contours (X and P increase from 0.1 to 0.9 upward and downward respectively) for a string in the presence of Kerr black hole. The mass of black hole is equal to 10, its rotation parameter is equal to 0 and horizon is located in $r_H = 20$.

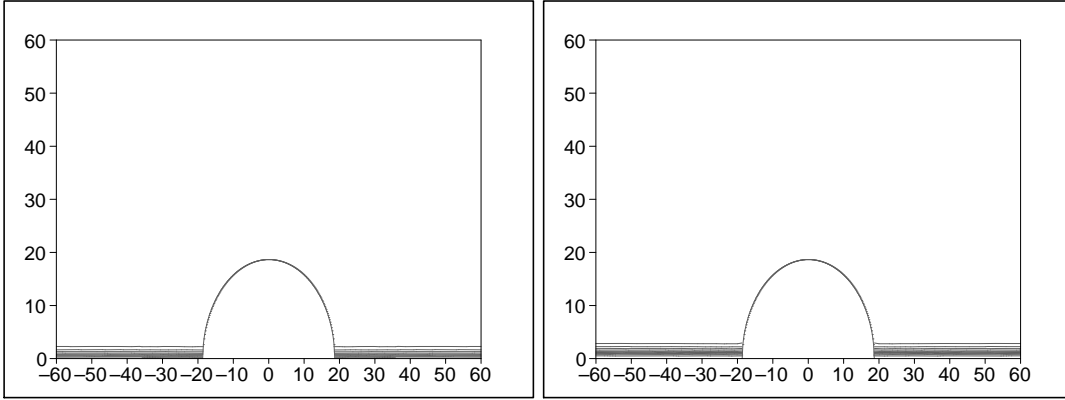


Figure 9: X and P contours (X and P increase from 0.1 to 0.9 upward and downward respectively) for a string in the presence of Kerr black hole. The mass of black hole is equal to 10, its rotation parameter is equal to 5 and horizon is located in $r_H = 18.66$.

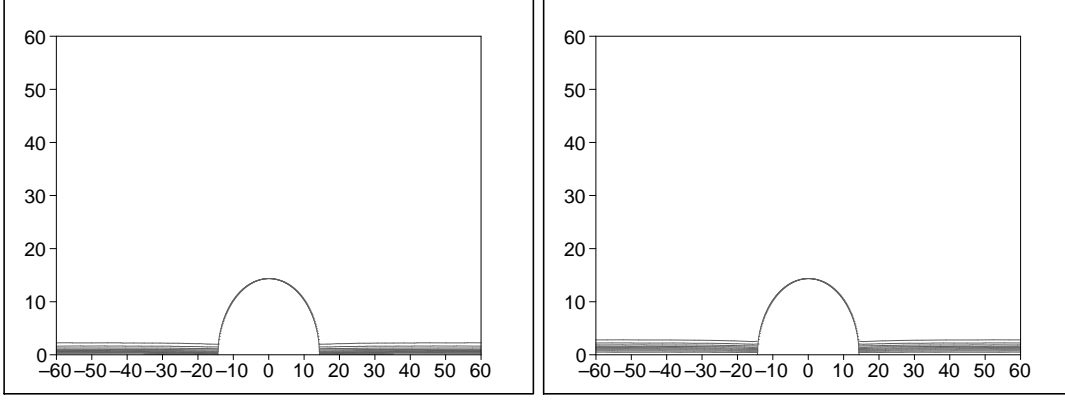


Figure 10: X and P contours (X and P increase from 0.1 to 0.9 upward and downward respectively) for a string in the presence of Kerr black hole. The mass of black hole is equal to 10, its rotation parameter is equal to 9 and horizon is located in $r_H = 14.36$.

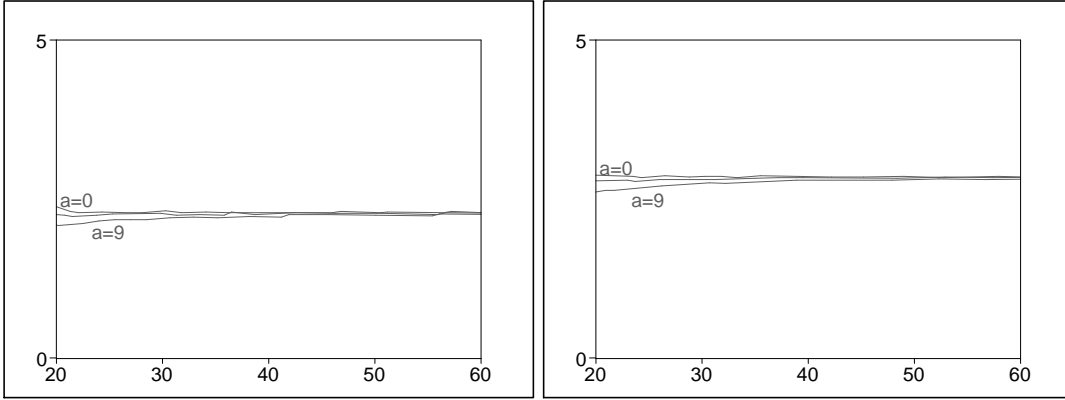


Figure 11: $X = 0.9$ and $P = 0.1$ contours in the Kerr black hole background of mass $m = 10$ for different values of the rotation parameter $a = 0, 5, 9$. The black hole horizon is located off to the left of the figure at $r_H = 20, 18.66, 14.36$ respectively.

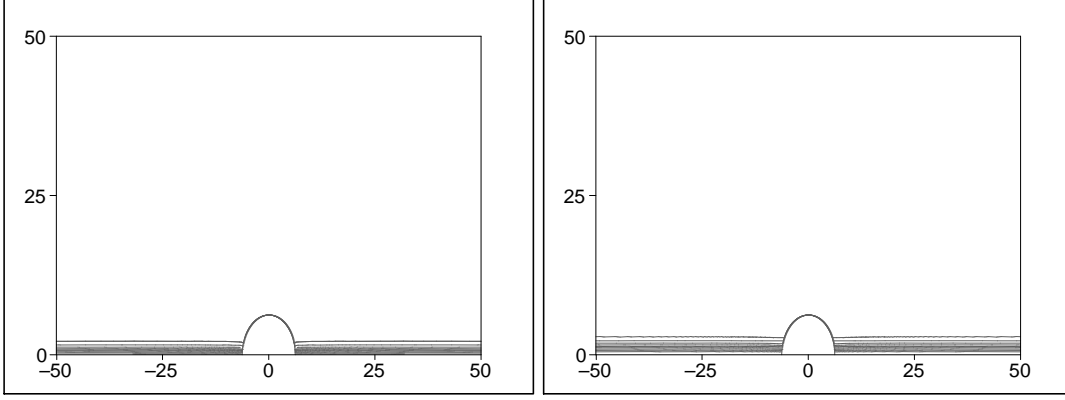


Figure 12: X and P contours (X and P increase from 0.1 to 0.9 upward and downward respectively) for a string in the presence of Reissner-Nordstrom-AdS black hole with $l = 5$. The mass of black hole is equal to 10, its charge parameter is equal to 5 and horizon is located in $r_H = 6.25$.

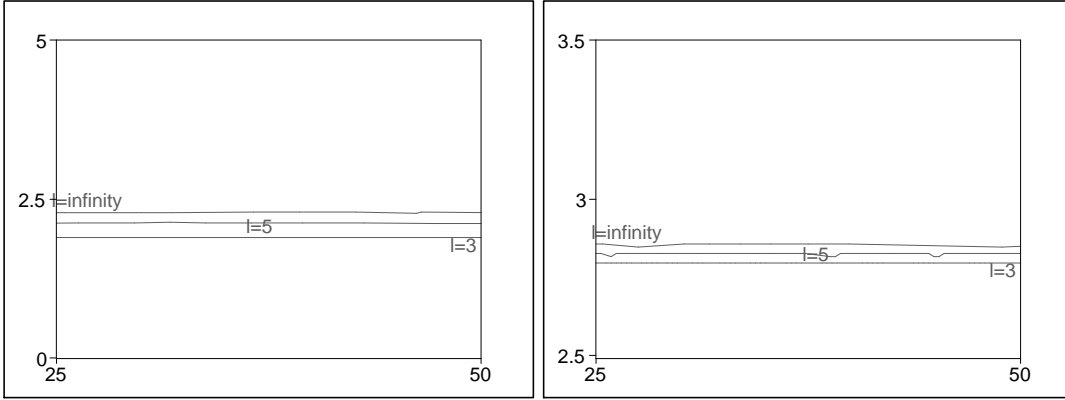


Figure 13: $X = 0.9$ and $P = 0.1$ contours in the Reissner-Nordstrom-AdS black hole background of mass $m = 10$ and charge $Q = 5$ for different values of the cosmological constant $l = 3, 5, \infty$. The black hole horizon is located off to the left of the figure at $r_H = 4.47, 6.25, 18.66$ respectively.

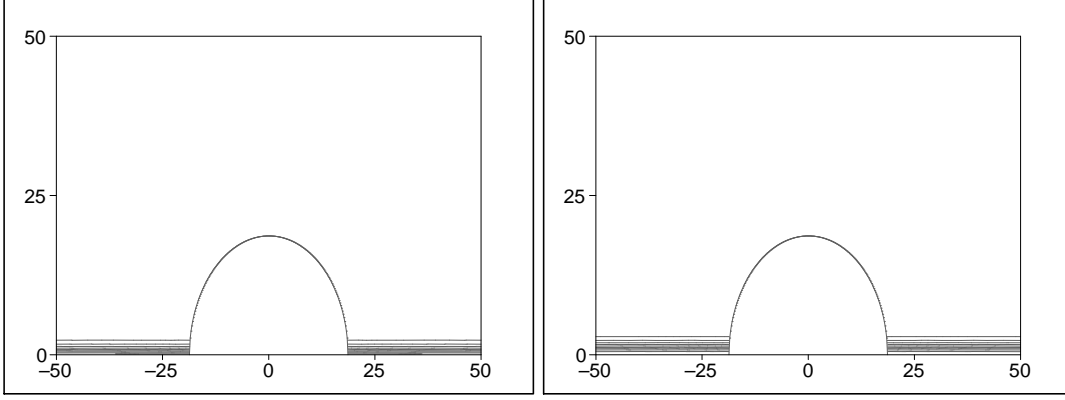


Figure 14: X and P contours (X and P increase from 0.1 to 0.9 upward and downward respectively) for a string in the presence of Reissner-Nordstrom black hole. The mass of black hole is equal to 10, its charge is equal to 5 and horizon is located in $r_H = 18.66$.

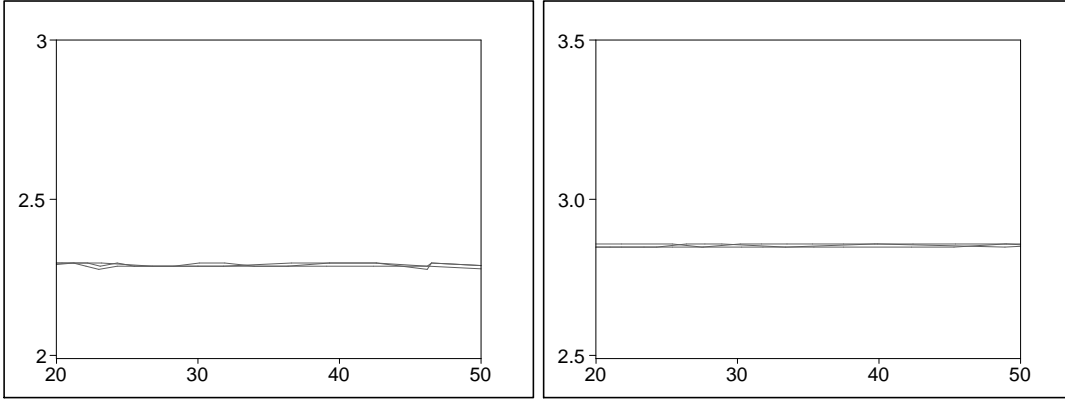


Figure 15: $X = 0.9$ and $P = 0.1$ contours in the Reissner-Nordstrom black hole background of mass $m = 10$ for different values of the charge $Q = 0, 5, 10$. The black hole horizon is located off to the left of the figure at $r_H = 20, 18.66, 10$ respectively.

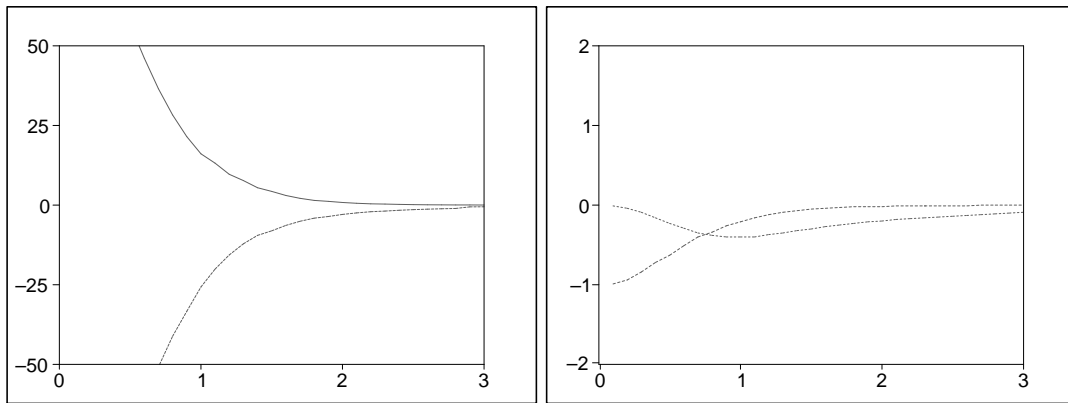


Figure 16: T_{tt} (solid), $T_{\theta\theta}$ (dashed), $T_{\varphi\varphi}$ (dotted) and T_{rr} (dot-dashed) curves versus ρ in $z = 8$ in the Kerr-AdS black hole background with $l = 5$. Winding number is $N = 1$.